Acta Neuropathologica
https://doi.org/10.1007/s00401-023-02596-8

ORIGINAL PAPER

From methylation to myelination: epigenomic and transcriptomic profiling of chronic inactive demyelinated multiple sclerosis lesions

Assia Tiane[1,2,3] · Melissa Schepers[1,2,3] · Rick A. Reijnders[2] · Lieve van Veggel[1,2,3] · Sarah Chenine[1,2,3] · Ben Rombaut[1,2,3] · Emma Dempster[4] · Catherine Verfaillie[5] · Kobi Wasner[6] · Anne Grünewald[6,7] · Jos Prickaerts[2] · Ehsan Pishva[2,4] · Niels Hellings[3,8] · Daniel van den Hove[2,9] · Tim Vanmierlo[1,2,3]

Received: 6 March 2023 / Revised: 1 June 2023 / Accepted: 1 June 2023

Abstract
In the progressive phase of multiple sclerosis (MS), the hampered differentiation capacity of oligodendrocyte precursor cells (OPCs) eventually results in remyelination failure. We have previously shown that DNA methylation of *Id2/Id4* is highly involved in OPC differentiation and remyelination. In this study, we took an unbiased approach by determining genome-wide DNA methylation patterns within chronically demyelinated MS lesions and investigated how certain epigenetic signatures relate to OPC differentiation capacity. We compared genome-wide DNA methylation and transcriptional profiles between chronically demyelinated MS lesions and matched normal-appearing white matter (NAWM), making use of post-mortem brain tissue ($n=9$/group). DNA methylation differences that inversely correlated with mRNA expression of their corresponding genes were validated for their cell-type specificity in laser-captured OPCs using pyrosequencing. The CRISPR–dCas9-DNMT3a/TET1 system was used to epigenetically edit human-iPSC-derived oligodendrocytes to assess the effect on cellular differentiation. Our data show hypermethylation of CpGs within genes that cluster in gene ontologies related to myelination and axon ensheathment. Cell type-specific validation indicates a region-dependent hypermethylation of *MBP*, encoding for myelin basic protein, in OPCs obtained from white matter lesions compared to NAWM-derived OPCs. By altering the DNA methylation state of specific CpGs within the promotor region of *MBP*, using epigenetic editing, we show that cellular differentiation and myelination can be bidirectionally manipulated using the CRISPR–dCas9-DNMT3a/TET1 system in vitro. Our data indicate that OPCs within chronically demyelinated MS lesions acquire an inhibitory phenotype, which translates into hypermethylation of crucial myelination-related genes. Altering the epigenetic status of *MBP* can restore the differentiation capacity of OPCs and possibly boost (re)myelination.

Keywords Epigenetics · Oligodendrocyte · Progressive MS · Epigenetic editing

Background

Multiple sclerosis (MS) is a demyelinating disease of the central nervous system (CNS), characterised by a variety of clinical symptoms, such as visual problems, fatigue, muscle stiffness, and cognitive impairment [34]. MS is defined by inflammation-induced demyelination during the early stages, which eventually results in gradual neurological disability as the disease progresses [34, 54].

During the progressive stages of MS, endogenous repair mechanisms (remyelination) become exhausted, resulting in the accumulation of chronically demyelinated lesions. Sustained demyelination within such lesions eventually causes loss of axonal density and neurodegeneration, which are two major contributors to the progressive nature of MS [41]. Even though the exact aetiology of progressive MS remains unclear, it is suggested that remyelination is hampered in these stages due to the inability of oligodendrocyte precursor cells (OPCs) to differentiate into mature myelinating oligodendrocytes [14]. Indeed, despite the abundant presence of OPCs within chronically demyelinated inactive MS lesions, their differentiation towards myelinating oligodendrocytes is attenuated in these demyelinated areas [17]. This suggests that OPCs within chronically demyelinated MS lesions

Daniel van den Hove and Tim Vanmierlo have contributed equally to this work.

Extended author information available on the last page of the article

Published online: 07 June 2023

acquire a quiescent phenotype, leading to a differentiation block and, thus, ineffective remyelination.

In support of this idea, it has been shown that OPC differentiation is highly dependent on epigenetic regulation, which can be easily influenced by external stimuli from the surrounding microenvironment, such as sustained inflammation and inhibitory factors of the extracellular matrix [8, 10, 29, 49, 52]. Epigenetic modifications are highly implicated in oligodendroglial biology [5, 43, 49]. DNA methylation, for instance, is a stable yet at the same time dynamic epigenetic mark that translates environmental stimuli to alterations in gene expression and subsequent cellular behaviour. We and others have previously shown that DNA methylation contributes to physiological OPC differentiation [36, 48]. In addition, DNA methylation is also required for remyelination, as shown in a mouse model for focal demyelination [37]. This suggests that in the context of progressive MS, disturbed DNA methylation patterns in the oligodendrocyte lineage might be an acquired underlying feature of remyelination failure. Despite many advances in the field of neuroepigenetics, the number of epigenome-wide association studies (EWAS) conducted on MS brain tissue is very limited. The majority of EWAS studies in MS have been performed on normal-appearing white matter (NAWM) samples, which revealed important changes in DNA methylation prior to myelin damage, but do not show the epigenetic state in actual demyelinated MS lesions, where OPCs acquire a quiescent phenotype resulting in impaired remyelination [23, 28, 30].

In the present study, we quantified epigenomic and transcriptomic profiles of chronically demyelinated inactive MS lesions and their surrounding NAWM to investigate which genes could underlie the differentiation block of OPCs within the lesion environment. Cell-specific validation in laser-captured OPCs showed that OPCs within the lesion exhibit a hypermethylated profile of essential myelin genes, such as *MBP*. By applying the CRISPR/dCas9-mediated epigenetic editing toolbox, we examined the causal relationship between the methylation of these myelin genes and the differentiation capacity of human-induced pluripotent stem cell (iPSC)-derived oligodendrocytes.

Materials and methods

Sample collection

Human post-mortem brain tissue was obtained from the Netherlands Brain Bank (http://www.brainbank.nl). Chronic, inactive demyelinated white matter lesions were selected from progressive MS patients ($n = 10$, one lesion per patient) and characterised for demyelination (proteolipid protein [PLP^-]), inflammation (human leukocyte antigen [$HLA\text{-}DR^-$], Oil Red O [ORO^-]), and presence of OPCs (neural/glial antigen 2 [$NG2^+$]) by immunohistochemistry [48]. Demographic details were described before [48]. Lesions were manually dissected from the surrounding NAWM, using the proteolipid protein (PLP) staining as a reference. Slices of 30 µM were made using a CM3050 S cryostat (Leica) and were alternately collected for either RNA or DNA isolation (Fig. 1a). For laser-capture microdissection and immunohistochemistry, slices of 10 µM were cut and collected on glass microscopy slides.

Transcriptomic profiling

Total RNA was extracted from lesions and their surrounding NAWM, using the RNeasy mini kit (Qiagen), according to the manufacturer's instructions. RNA concentrations were analysed with a Nanodrop spectrophotometer (Isogen Life Science). RNA integrity was checked using the Agilent RNA 6000 Pico Bioanalyzer (Agilent Technologies). RNA integrity number (RIN) values ranged between 2.40 and 6.70. Samples (500 ng per sample) were processed and sequenced by the Genomics Core Leuven (Leuven, Belgium). Library preparation was performed using the Lexogen 3′mRNA-Seq Library Prep Kit (Isogen Life Science). Libraries were sequenced on the Illumina HiSeq4000 sequencing system. Reads per sample ranged from 9 to 15 million reads and quality control (QC) of raw reads was performed with FastQC v0.11.7 [1]. Adapters were filtered with ea-utils fastq-mcf v1.05 [2]. Using the default parameters, splice-aware alignment was performed with HISat2 against the human reference genome hg38 [24]. Reads mapping to multiple loci in the reference genome were discarded. The resulting BAM alignment files were handled with Samtools v1.5 [32]. Read counts for each gene were compiled using Rsubread (version 2.8.2) by reading in and processing each bam file. A minimum threshold of 15 counts-per-million reads for at least 40% of all samples was used to determine whether a gene was expressed, leaving 8399 genes for analysis. The package EdgeR (version 3.36.0) was used to normalise and transform counts to log counts-per-million, using the Trimmed Mean of M-values (TMM) normalisation method. Differential expression analysis was performed using the *limma* package (version 3.50.0) [42]. Age, sex, and post-mortem interval (PMI) were included as covariates and individual was treated as a random intercept, using the *duplicateCorrelation* function from the *limma* package. *P* values were FDR-corrected for multiple testing to determine differentially expressed genes (DEG, FDR p value < 0.05 and absolute fold change > 1.5) between lesion and NAWM samples.

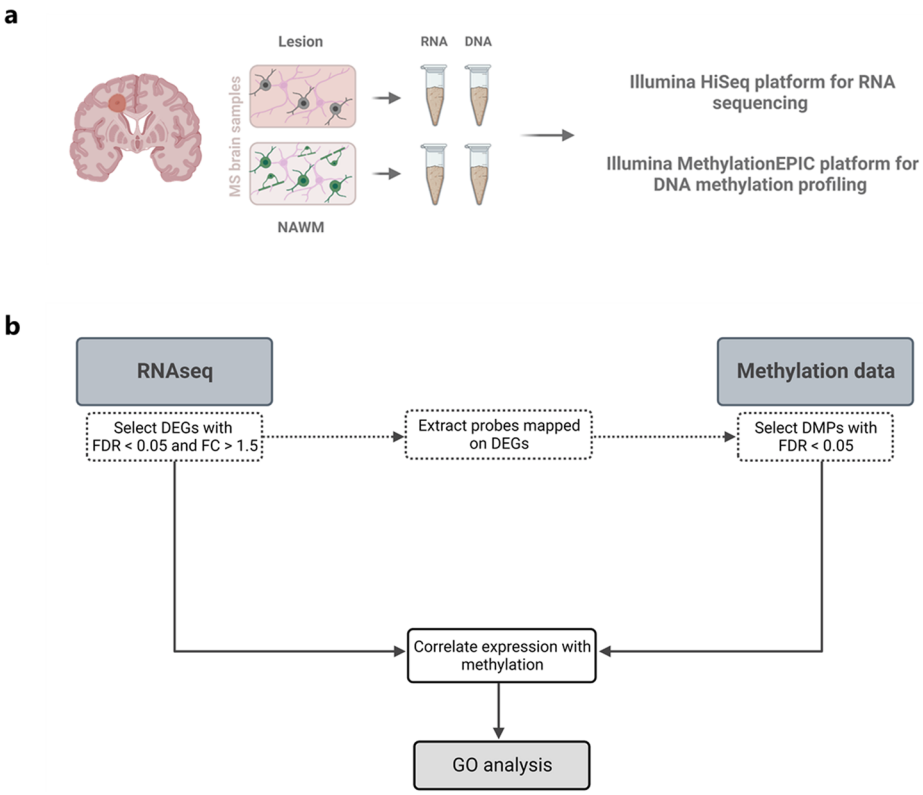

Fig. 1 Overview of the sample preparation and data analysis workflow. **a** Multiple sclerosis (MS) lesions and surrounding normal-appearing white matter (NAWM) were dissected and both were collected for RNA and DNA isolation. Transcriptomic and methylomic profiling was carried out using the HISeq sequencing and Illumina MethylationEPIC array platform, respectively. **b** Illustration of the data analysis workflow integrating the transcriptomic and methylomic datasets. *NAWM* normal-appearing white matter, *DEGs* differential expressed genes, *FDR* false discovery rate adjusted *p* value, *FC* fold change, *DMPs* differential methylated probes, *GO* gene ontology

Methylomic profiling

Genomic DNA was extracted using a standard chloroform–phenol extraction and ethanol precipitation method. DNA concentration was assessed with the Qubit dsDNA HS Assay Kit (Invitrogen). A minimum of 500 ng per sample was used for the Illumina Infinium MethylationEPIC array BeadChip (850K), which was carried out by the Epigenomic Services from Diagenode (Liège, Belgium; Cat nr. G02090000). The DNA was deaminated with the EZ-96 DNA Methylation Kit (Zymo Research) according to Illumina's recommended deamination protocol. Methylation data processing and statistical analyses were performed using the programming language R (version 4.1.2.) and RStudio (version 2021.09.1). Raw IDAT files were loaded into R using the minfi package [3]. To confirm that matched lesion and NAWM samples were from the same individual, we made use of 59 single-nucleotide polymorphism (SNP) probes on the Illumina EPIC array to cluster genetically identical samples. Cell proportion estimates were generated using the Houseman method [21]. Samples with a $NeuN^+$ estimation of more than 5% were excluded from the analysis. Cross-hybridising probes and probes containing SNPs were removed [35]. Probe filtering was performed using the *pfilter* function from the wateRmelon package (version 2.0.0) to exclude probes with > 1% of samples with a detection *p* value > 0.05 [40]. The remaining data were normalised using the *dasen* function from the wateRmelon package, and probes on the X and Y chromosomes were excluded from the dataset. As principle component analysis (PCA) trait analysis showed a significant correlation with the EPIC chip IDs, we corrected for this batch effect using the *ComBat* function from the *sva* package (version 3.20.0), which applies a Bayesian method to adjust for known batch covariates [31]. After data processing, eight lesion and nine NAWM samples remained, as well as 769,804 probes.

We extracted all the beta values of the CpG probes from the Illumina methylationEPIC array that were annotated (Illumina UCSC annotation) to DEGs from the RNAseq analysis. Out of the 769,804 probes, 29,446 probes were used as input for the differential methylation analysis using the same approach as for the DEG analysis. The *duplicateCorrelation* function from the *limma* package was applied to block individual as a random effect. Age, sex, and PMI were included as covariates in the regression model, and FDR correction for multiple testing was applied to the nominal *p* values to identify differentially methylated probes (DMPs, FDR *p* value < 0.05).

All DE genes that contained a DMP were subjected to a Pearson's correlation analysis between expression (LogCPM) and methylation (bèta values) levels of each differentially methylated CpG within that gene. A final list of genes that displayed differential expression and methylation, and a significant correlation between both expression and

methylation, was used as input for a gene ontology (GO) analysis using the *enrichGO* function from the *clusterProfiler* package (version 4.2.2), focussing on the 'Biological Process' ontologies. An overview of the data analysis workflow is provided in Fig. 1b.

Laser-capture microdissection

OPCs were stained using an accelerated protocol to maintain DNA integrity. Briefly, sections were fixed in ice-cold acetone for 10 min and dip-washed in TBS/TBS-T/TBS. Endogenous peroxidase activity was neutralised with 1.5% H_2O_2 in TBS for 10 s, followed by a rinse with TBS and a 30-min blocking step with the Dako Protein Block (Dako) at room temperature. The slices were incubated with a primary antibody against NG2 (1:200, Abcam Ab101807) for 30 min, followed by a quick wash step in TBS. Sections were incubated with horseradish peroxidase (HRP)-conjugated EnVision + Dual Link System (Dako) for 15 min, washed with TBS, and incubated with an avidin-biotinylated horseradish peroxidase complex for 10 min, after which visualisation of the staining was accomplished using 0.3% ammonium nickel sulphate and 0.025% diaminobenzidine (pH 7.8) in TBS. After sequential dehydration steps (30 s in 75%–95%–100% ethanol and 5 min in xylene), the samples were ready for immediate laser-capture microdissection using a PALM MicroBeam (Zeiss). 50 cells were isolated per region and collected into 0.1 ml tube caps containing 10 µl PBS and used for pyrosequencing.

CRISPR–dCas9 plasmids

Guide design

A specific single guide RNA (sgRNA) was designed to induce (de)methylation within the promoter region of the *MBP* (chr18:74,690,791–74,691,721) gene using Benchling software (Supplementary Information S1). Off-target sites were predicted using the CRISPR–Cas9 guide RNA design checker from Integrated DNA Technologies (IDT). Guides were synthesised as oligos with overhangs to fit into the BbsI restriction gap and an additional guanine for increased transcriptional efficiency.

sgRNA cloning

Guides were cloned into the DNMT3a plasmids (Addgene #71667 and #71684) using a one-step digestion and ligation protocol. Briefly, 100 ng of plasmid was added to a mixture of 1 µM of the annealed guide oligos, 20 U BbsI restriction enzyme (Bioké), 1 × cutsmart buffer (Bioké), 400 U T4 ligase (Bioké), 1 × T4 ligase buffer (Bioké), and H_2O to an end volume of 20 µl, and incubated for 30 cycles of 5 min on 37 °C and 5 min on 23 °C. The product was then transformed into NEB 5-alpha Competent *E. coli* cells (Bioké) and plated on LB-agar plates, supplemented with ampicillin (Amp; 100 mg/ml). Suitable colonies were propagated overnight in LB-Amp medium. Plasmids were extracted using the NucleoBond Xtra Midi kit, according to the manufacturer's protocol (Macherey-Nagel). Sanger sequencing was carried out on purified plasmid vector to validate the sgRNA incorporation. For the TET1 vectors (Addgene #129025 and #129026), we performed subcloning from the DNMT3a vectors using the PvuI and XbaI restriction enzymes (Thermofisher). One µg of each vector was incubated overnight at 37 °C with 10 U of both restriction enzymes, 1 × Tango buffer, and H_2O up to a total volume of 50 µl. The samples were loaded on an agarose gel (1%) and both insert (from the DNMT3a vectors), as well as vectors (from the TET1 vectors) were extracted from the gel, using the PCR and gel clean-up kit (Macherey-Nagel) according to the manufacturer's instructions. Inserts and vectors were ligated with the T4 DNA Ligase buffer and enzyme system (Bioké) into the linearized vector in a 2:1 insert-to-vector molar ratio. Plasmid transformation and purification was performed as described above.

Human-derived iPSC-oligodendrocytes

Cell culture

Inducible SOX10-overexpressing iPSCs were used to generate O4+ and MBP+ oligodendrocyte cultures as described previously and kindly provided under a material transfer agreement (MTA) by Catherine Verfaillie (KuLeuven, Leuven, Belgium) [16, 39]. Differentiated iPSC-oligos were frozen in liquid nitrogen and thawed for transfection experiments. For differentiation assays, cells were seeded at a density of 250,000 cells/well in a PLO/laminin-coated 24-well plate and maintained in differentiation medium with doxycycline (4 µg/ml). For microfiber myelination assays, cells were seeded at a density of 50,000 cells/scaffold on PLO/laminin-coated aligned PLLA 2 µm-diameter fibre scaffold substrates and maintained in differentiation medium with doxycycline (4 µg/ml) [4].

Transfection

The DNMT3a plasmids were a gift from Vlatka Zoldoš (Addgene #71667 and #71684), and the TET1 plasmids were a gift from Julia K. Polansky (Addgene #129025 and #129026). Plasmids were transfected into human iPSC-derived OPCs 48 h after seeding, using the OZ Biosciences NeuroMag Transfection Reagent (Bio-connect), following the manufacturer's instructions. In brief, 1 µg of plasmid DNA was diluted in 50 µl DMEM/F12 medium,

added to 1.75 µl NeuroMag reagent, and incubated for 20 min at room temperature. DNA/NeuroMag complexes were dropwise added to iPSC-oligo cultures, maintained in differentiation medium, and placed on a magnetic plate for 4 h in a 5% CO_2 incubator. Medium change with fresh differentiation medium, containing doxycycline (4 µg/ml), was performed 72 h after transfection. Cells were lysed or fixated on day 5 post-transfection for assessing cellular differentiation or on day 12 post-transfection for the myelination assay.

Human oligodendroglioma (HOG) cell line

The human oligodendroglioma cell line HOG was maintained in culture medium (DMEM, 10% FCS, 1% P/S) at 37 °C and 5% CO_2. For transfection experiments, cells were seeded in poly-L-lysine (PLL, Sigma-Aldrich)-coated 24-well plates at a density of 37,500 cells per well. After attaching to the plate, cells were transfected on the same day as the seeding, using the protocol described above, with a minor adjustment (3 µl NeuroMag reagent and 500 ng DNA per well for 30 min on the magnetic plate). Cells were maintained in differentiation medium (DMEM, 1% P/S, 0.05% FCS, 5 µg/ml bovine insulin, 5 µg/ml transferrin, 0.03 nM sodium selenite, and 30 nM L-thyroxine; all from Sigma-Aldrich), with one medium change 48 h after transfection. On day 4 post-transfection, cells were fixated for further experiments.

Pyrosequencing

Genomic DNA was extracted from laser-captured OPCs, as well as transfected iPSC-OPCs, and bisulfite-converted, using the Zymo Research EZ DNA Methylation-Direct Kit (BaseClear Lab Products). PCR primers were designed using the PyroMark Assay Design 2.0 software (Qiagen, Supplementary Information S2). The assay for *MBP* was tested for its sensitivity using the EpiTect PCR Control DNA Set (Qiagen). Product amplification was performed using the following reaction mixture: 1 × buffer with 20 mM $MgCl_2$ (Roche), 10 mM dNTP mix (Roche), 5 µM forward and reverse primers (Metabion AG), 1 U FastStart Taq DNA Polymerase (Roche), bisulfite-converted DNA, and nuclease-free water to a total volume of 25 µl. PCR cycling was performed as follows: initial denaturation for 5 min at 95 °C, 50 cycles of 30 s at 95 °C, 30 s at 60 °C, and 1 min at 72 °C; final extension for 7 min at 72 °C. PCR amplicons were sequenced using the Pyromark Q48 instrument (Qiagen) with the PyroMark Q48 Advanced CpG Reagents (Qiagen), according to the manufacturer's protocol and quantified with the Pyromark Q48 Autoprep software.

Quantitative PCR

Transfected iPSC-OPCs and post-mortem human MS samples were lysed in Qiazol (Qiagen), and RNA was isolated using a standard chloroform extraction and ethanol precipitation method. RNA concentration and quality were analysed with a Nanodrop spectrophotometer (Isogen Life Science). RNA was reverse-transcribed using the qScript cDNA Supermix kit (Quanta). qPCR was performed to analyse gene expression using the Applied Biosystems QuantStudio 3 Real-Time PCR System (Life Technologies). The reaction mixture consisted of SYBR Green master mix (Life Technologies), 10 µM forward and reverse primers (Integrated DNA Technologies), nuclease-free water, and cDNA template (12.5 ng), up to a total reaction volume of 10 µl. The primers used for amplification are listed in Supplementary Information S3. Start fluorescence values were calculated for the human MS sample validation of the RNAseq data. Transfection results were analysed by the comparative Ct method and were normalised to the most stable housekeeping genes (RPL13a and TBP).

Immunocytochemistry

Transfected cells were fixed in 4% paraformaldehyde (PFA) for 30 min at room temperature. Aspecific binding was blocked for 30 min with 1% bovine serum albumin (BSA) in 0.1% PBS-T, followed by incubation with primary antibodies (Supplementary Information S4) for 4 h at room temperature. After three washing steps with PBS, cells were incubated with Alexa 488- or Alexa 555-conjugated secondary antibody (Supplementary Information S4) for 1 h. Nuclei were counterstained with 4′6-diamidino-2-phenylindole (DAPI; Sigma-Aldrich). Coverslips were mounted with Dako mounting medium (Dako) and analysed using a fluorescence microscope (Leica DM2000 LED). Per coverslip, three images were quantified using Fiji ImageJ software.

Statistical analysis

Statistical analysis of the transfection and pyrosequencing experiments was performed using GraphPad Prism 9.0.0 software (GraphPad software Inc., CA, USA). Differences between group means within these experiments were determined using an unpaired *t* test for normally distributed data and a Mann–Whitney test for not normally distributed data. Differences in methylation at different CpG sites were determined using a two-way repeated-measures ANOVA with Šídák's multiple comparisons test. All data are depicted as mean ± SEM, $*p \leq 0.05$, $**p < 0.01$, $***p < 0.001$, $****p < 0.0001$.

Results

Transcriptomic profiling of chronic inactive demyelinated MS lesions and the surrounding NAWM

Bulk RNA sequencing was performed on chronically demyelinated MS lesions and the corresponding surrounding NAWM. After stringent data pre-processing and QC filtering, 17 samples (9 lesions and 8 NAWM) were included in the RNA data analysis. Gene clustering based on absolute expression levels indicated clustering of the lesions separately from the NAWM (Fig. 2a). Interestingly, lesions and NAWM that cluster close to each other were derived from the same individual. PCA based on the logCPM values showed that 63% of the variance could be explained by PC1, which highly correlated ($p = 0.00059$) with the sample group (Fig. 2b). Out of the total of 8399 genes that were subjected to a differential gene expression analysis, 641 genes were found to be significantly differentially expressed between lesion and NAWM, with an absolute fold change above 1.5 (Fig. 2c, Supplementary Table 1). Interestingly, the distribution was roughly balanced between upregulated (242) and downregulated (399) genes.

Genes involved in glial cell development and myelination are differentially methylated in chronic MS lesions

The Illumina methylationEPIC array was used to analyse the DNA methylation state of the chronically demyelinated lesions and NAWM samples. PCA revealed clustering of the samples based on the methylation bèta values, similar to those observed in the RNA sequencing data (Fig. 3a). Out of the 769,804 CpGs that passed the initial quality control, 29,446 CpG sites were annotated to the DEGs from the transcriptome analysis. Differential methylation analysis of these genes showed that 8336 CpG positions were significantly (FDR p value < 0.05) differentially methylated between lesions and NAWM (Fig. 3b, Supplementary Table 2). Each of these differentially methylated positions (DMPs) were then subjected to a correlation analysis with the matching expression data. Interestingly, 512 genes showed a significant (FDR-adjusted p value < 0.05) and strong correlation between their expression and methylation profile (Supplementary Table 3). Figure 3c shows the top ten correlating CpGs, nine of which showing a strong negative correlation between DNA methylation and RNA expression. The final set of 512 genes, which were differentially expressed, differentially methylated and correlated between both expression and methylation of at least one CpG, was used for the GO analysis, with a focus on Biological Process (Fig. 3d). Clustering of the significantly enriched GO terms showed two main clusters, related to glial cell development/myelination and cytoskeleton organisation (Fig. 3d).

As we are particularly interested in the contribution of DNA methylation to (re)myelination in the MS lesions, we focussed on the genes that were part of the enriched GO clusters related to glial cell development/myelination (GO:0021782, GO:0007272, GO:0008366, and GO:0042552). We explored the distribution of those DMPs across gene features (Fig. 4a) and CpG-related island features (Fig. 4b). Interestingly, the gene *MBP*, coding for myelin basic protein, the second most abundant protein in central nervous system myelin, did contain the highest number of DMPs in general as well as the highest number of DMPs that were located in the promotor region (TSS1500, TSS200)

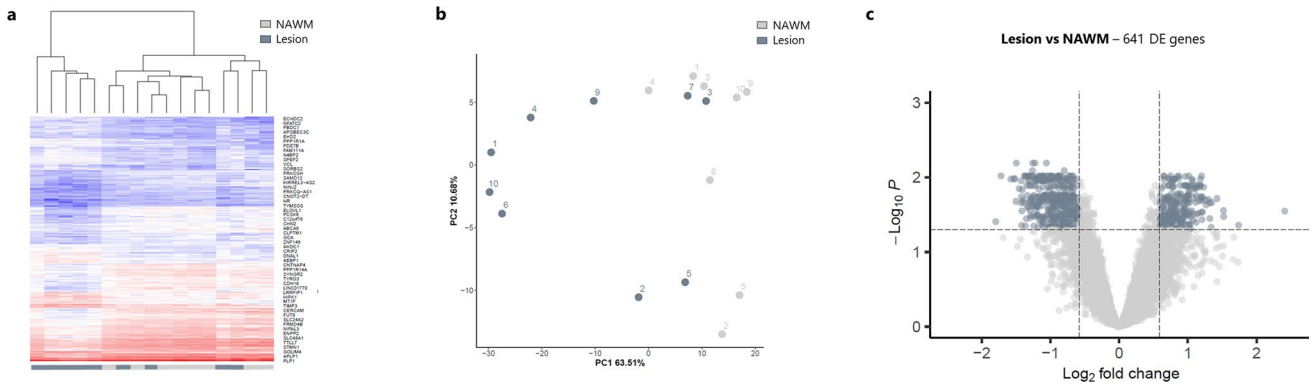

Fig. 2 Chronically demyelinated lesions are transcriptionally distinct from the surrounding normal-appearing white matter (NAWM). Based on the transcriptomic profile, chronic multiple sclerosis (MS) lesions can be distinguished from the surrounding NAWM, as determined by **a** gene clustering based on absolute expression levels and **b** a principal component analysis (PCA). The numbers in the PCA plot represent the donors to highlight which lesions and NAWM are derived from the same patient. **c** Differential expressed genes (DEGs) analysis revealed 641 genes that are significantly differentially expressed between lesion and NAWM (FDR p value < 0.05), with an absolute fold change above 1.5

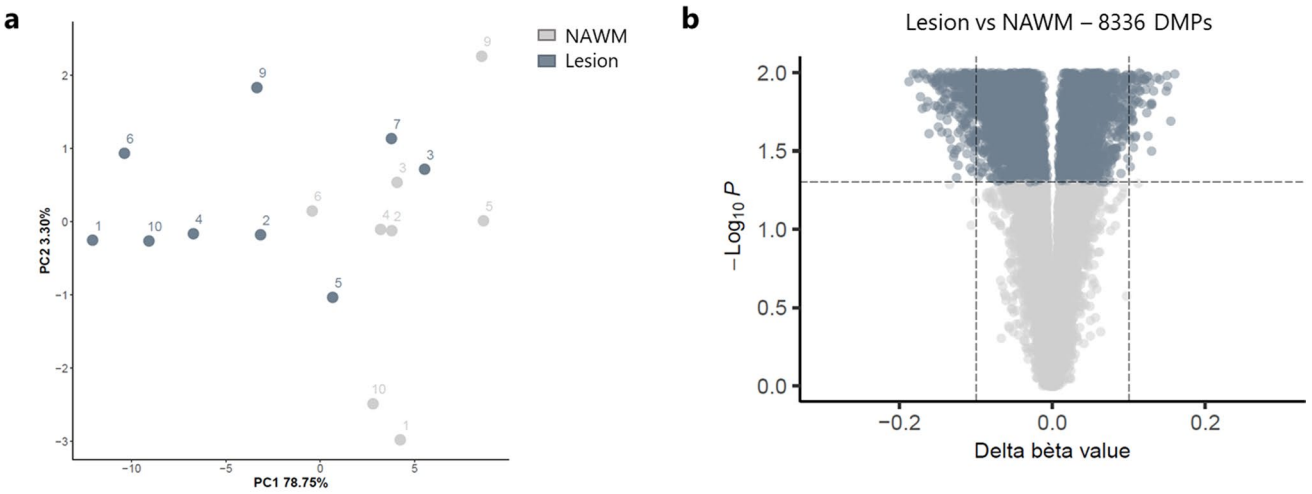

c

Probe ID	Gene	Pearson's *r*	P-value	FDR adjusted p-value	CpG feature
cg12139813	BTBD3	-0.959	1.23E-09	5.11E-06	Body
cg23017573	PIP4K2A	-0.960	1.01E-09	5.11E-06	Body
cg14541848	SEMA4D	-0.955	2.73E-09	7.58E-06	Body
cg23874669	DDR2	0.949	6.64E-09	1.29E-05	TSS1500;Body
cg12126243	DAAM1	-0.946	1.03E-08	1.29E-05	Body
cg19094243	TMEFF2	-0.945	1.09E-08	1.29E-05	Body
cg23644066	RNF220	-0.947	8.09E-08	1.29E-05	TSS1500
cg02249322	PCSK6	-0.942	1.62E-08	1.64E-05	Body
cg16100530	SH3GL3	-0.942	1.62E-08	1.64E-05	Body
cg26360766	LPAR1	-0.938	2.59E-08	2.34E-05	Body

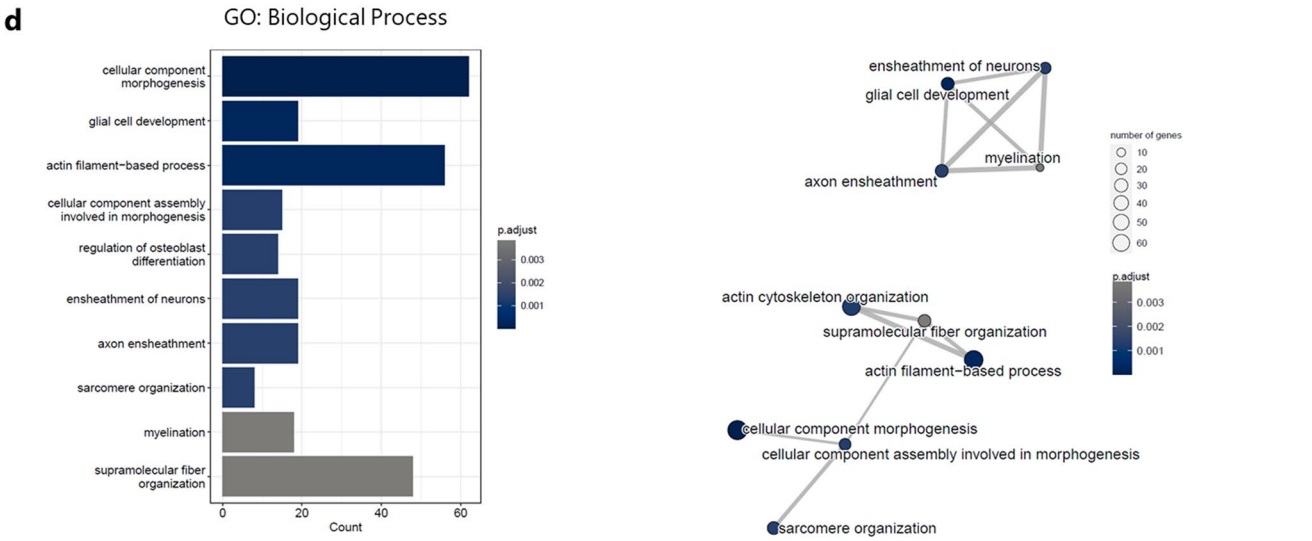

Fig. 3 Differentially methylation analysis between lesions and NAWM reveals enriched gene ontologies (GOs) related to glial cell development and myelination. **a** Principal component analysis (PCA) shows the clustering of the samples based on the methylation bèta values. The numbers in the PCA plot represent the donors to highlight which lesions and NAWM are derived from the same patient. **b** Out of the 29,446 analysed CpG sites, 8336 CpGs are differentially methylated between lesions and normal-appearing white matter (NAWM; FDR < 0.05). **c** Pearson's correlation analysis between methylation and expression levels of the significantly differentially methylated CpGs. **d** Gene ontology analysis of the 512 genes that were differentially expressed and correlated significantly with their differential methylated probes (DMPs) revealed two main significantly enriched clusters related to the cytoskeleton and glial cell development/myelination

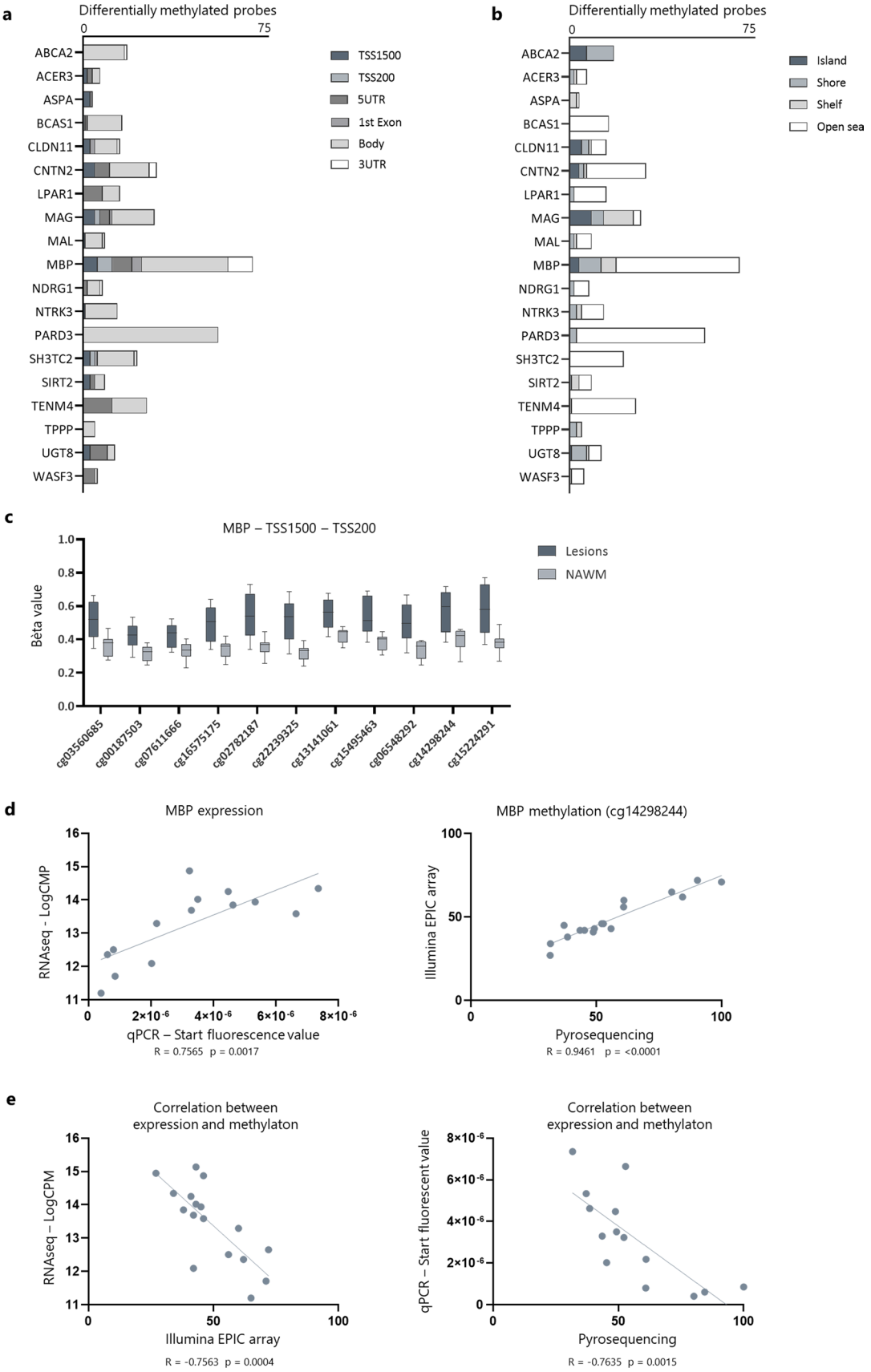
a
Differentially methylated probes
0
75
ABCA2
ACER3
ASPA
BCAS1
CLDN11
CNTN2
LPAR1
MAG
MAL
MBP
NDRG1
NTRK3
PARD3
SH3TC2
SIRT2
TENM4
TPPP
UGT8
WASF3
TSS1500
TSS200
5UTR
1st Exon
Body
3UTR
b
Differentially methylated probes
0
75
Island
Shore
Shelf
Open sea
c
MBP – TSS1500 – TSS200
Lesions
NAWM
Bèta value
1.0
0.8
0.6
0.4
0.2
0.0
cg03560685
cg00187503
cg07611666
cg16575175
cg02782187
cg22239325
cg13141061
cg15495463
cg06548292
cg14298244
cg15224291
d
MBP expression
RNAseq - LogCMP
qPCR – Start fluorescence value
R = 0.7565 p = 0.0017
MBP methylation (cg14298244)
Illumina EPIC array
Pyrosequencing
R = 0.9461 p = <0.0001
e
Correlation between expression and methylaton
RNAseq – LogCPM
Illumina EPIC array
R = -0.7563 p = 0.0004
Correlation between expression and methylaton
qPCR – Start fluorescent value
Pyrosequencing
R = -0.7635 p = 0.0015

◂**Fig. 4** In-depth overview of the genes that are part of the enriched GO clusters related to glial cell development/myelination (GO:0021782, GO:0007272, GO:0008366, and GO:0042552). Distribution of DMPs within the GO clusters related to myelination across gene features (**a**) and CpG-related island features (**b**). The height of the bars represents the number of DMPs annotated to the gene. **c** The beta values of the DMPs located in the promoter region (TSS1500, TSS200) of *MBP* indicate consistent hypermethylation within lesions compared to the surrounding NAWM. **d** Technical validation of the expression and methylation levels of MBP, as determined by qPCR and pyrosequencing, respectively. Pearson's correlation analysis shows a significant correlation between both techniques on the expression level, as well as DNA methylation level ($n = 14$). **e** Expression and methylation levels of *MBP* (cg14298244) are significantly negatively correlated (Pearson's correlation analysis), both for array-based techniques (RNAseq, Illumina EPIC array), as well as targeted techniques (qPCR, pyrosequencing) ($n = 14$)

(Fig. 4a). An essential portion of these DMPs was furthermore situated in CpG islands or shores (Fig. 4b). Interestingly, all the CpGs within the promotor region of the gene were consistently hypermethylated in lesions compared to the surrounding NAWM (Fig. 4c). To technically validate our findings from the RNAseq and EWAS data, we performed targeted analysis of the expression and methylation profile of *MBP* using qPCR and pyrosequencing, respectively, in the same samples as used for the RNAseq and Illumina array. The correlation analyses for both expression and methylation showed a strong and significant correlation between the two techniques, serving as a robust validation of the RNA sequencing and EWAS discovery data (Fig. 4d). Furthermore, we observed a significant negative correlation between *MBP* expression and methylation levels (Fig. 4e). Altogether, these data suggest an important role of DNA methylation for the regulation of *MBP* expression.

Cell type-specific validation indicates hypermethylation of *MBP* in OPCs obtained from lesions, compared to NAWM-derived OPCs

The methylation signature within MS lesions suggests a potential differentiation and (re)myelination block, directly acting on essential myelin genes, such as *MBP*. However, as the Illumina EPIC array was performed on bulk tissue, the observed degree of methylation of *MBP* could also be explained by cellular heterogeneity of the samples. As we were particularly interested in whether there is a contribution of OPCs to the observed epigenetic signature of *MBP*, we stained OPCs within the samples, laser-capture micro-dissected, and collected them for targeted methylation analysis of the *MBP* promotor region by means of pyrosequencing (Fig. 5a). In line with our bulk tissue findings, we again observed a hypermethylated profile in OPCs obtained from lesions compared to OPCs that were located in the NAWM (Fig. 5b, c).

Targeted epigenetic editing of the *MBP* gene influences the differentiation capacity of human oligodendroglioma cells and human iPSC-derived oligodendrocytes

As we discussed elaborately in our recently published perspective [25], most EWAS observations remain correlational, making it difficult to infer a cause–effect relationship. In the last couple of years, epigenetic editing, i.e., altering the epigenome by directing, e.g., DNA methylation at a specific site, has grown as a powerful tool to further study the role of epigenetics in health and disease, especially in view of addressing causality. Hence, we applied CRISPR–dCas9-based epigenetic editing to investigate potential cause-and-effect relationships for epigenetic alterations of *MBP* regarding oligodendrocyte differentiation. A sgRNA was designed to target the promotor region of *MBP* and cloned into CRISPR–dCas9-DNMT3a or CRISPR–dCas9-TET1 vectors, to, respectively, methylate or demethylate the CpG sites within the *MBP* promotor region. As the off-target effects, due to unspecific binding of the sgRNAs, still remain an ongoing challenge in the field of epigenetic editing, we used an online tool to predict possible off-target site of our sgRNA. All the predicted off-target sites were located in non-coding genomic regions of the DNA (Supplementary Information S5).

We transfected a human oligodendroglioma (HOG) cell line with the epigenetic editing vectors (Fig. 6a). We observed an increased cellular complexity and MBP fluorescence area in cells transfected with the TET1 construct, and decreased MBP area in DNMT3a-transfected cells, suggesting an important role of *MBP* methylation on cellular differentiation (Fig. 6b, c). As the HOG cell line is not fully representative of human oligodendrocytes, we also explored the impact of epigenetic editing on human iPSC-derived oligodendrocytes. Similar to the HOG cells, iPSC-derived oligodendrocytes transfected with an active TET1 construct targeting the *MBP* promotor showed increased MBP protein expression (as determined by the MBP-positive area per transfected cell) (Fig. 7a, b). Human iPSC-derived oligodendrocytes that were transfected with the DNMT3a construct to methylate the *MBP* promotor showed a tendency towards decreased MBP expression (Fig. 7a, b). To evaluate the differentiation capacity of the transfected cells, we furthermore performed a Sholl analysis (Fig. 7c–f). Analysis of the ending radius (Fig. 7d), the sum of intersections (Fig. 7e) and the average number of intersections per Sholl ring (Fig. 7f) all showed that modulation of the *MBP* promotor methylation status influences cellular differentiation. Furthermore, as increased MBP protein expression and oligodendrocyte differentiation does not necessarily mean increased myelination, we also performed a myelination assay using neuron-free 3D microfibers (Fig. 7g). We also observed increased length of the process extensions covering the microfibers in the

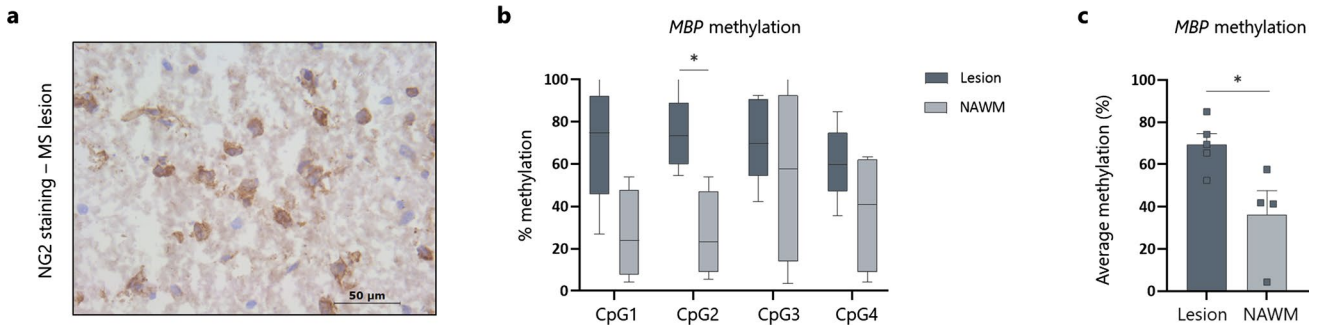

Fig. 5 Cell-specific validation of the hypermethylated profile of *MBP* within OPCs derived from lesions, compared to OPCs isolated from the surrounding NAWM. **a** OPCs were stained for the NG2 marker and laser-capture micro-dissected from either lesions of NAWM. Batches of 50 cells per sample were subjected to bisulfite pyrosequencing to determine the methylation profile of the *MBP* promoter region. **b**, **c** OPCs within the promoter region of *MBP* show a hypermethylated profile compared to OPCs isolated from the NAWM ($n = 4$–5, two-way ANOVA with Šídák's multiple comparisons test for **b** and Wilcoxon test for **c**). Data are represented as mean ± SEM, $^*p < 0.05$

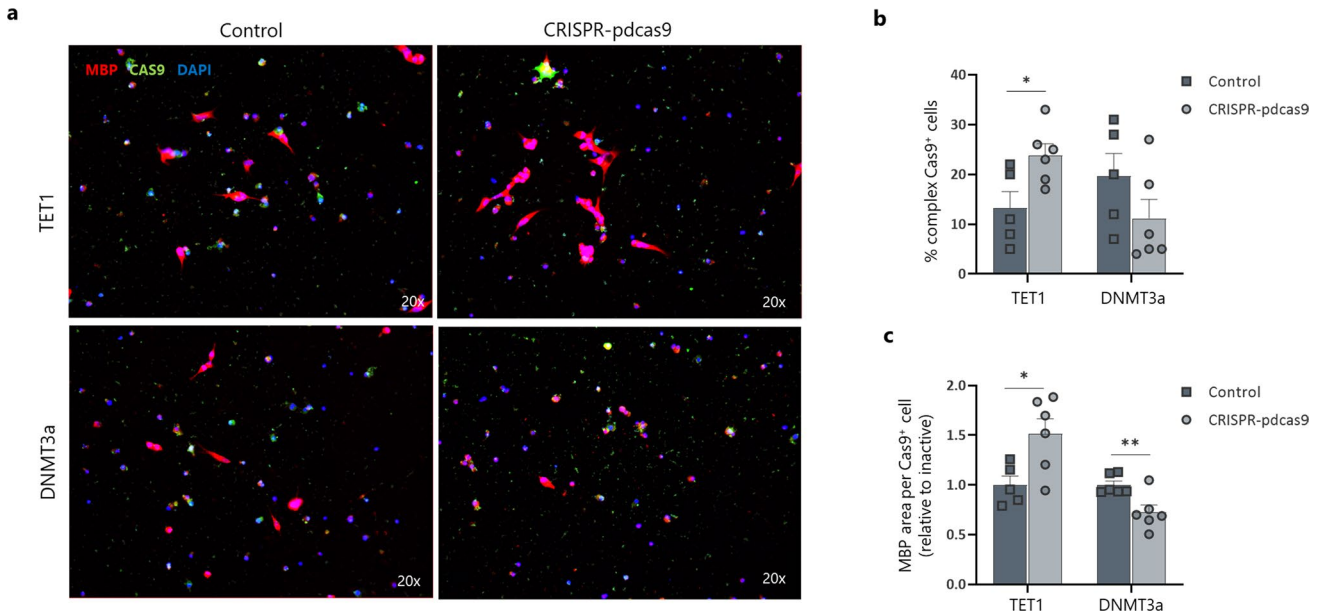

Fig. 6 Epigenetic editing of the *MBP* promotor region in a human oligodendroglioma (HOG) cell line influences cellular complexity. HOG cells were transfected with either a CRISPR–pdCas9-DNMT3a or CRISPR–pdCas9-TET1 vector to methylate or demethylate the promotor region of the *MBP* gene. Inactive constructs harbouring a catalytical inactive DNMT3a or TET1 were used as control. **a**–**c** Representative images and quantification (complexity and MBP fluorescence area) of transfected human oligodendroglioma cells show an impact of epigenetic editing on cellular behaviour ($n = 6$, unpaired t test). Data are represented as mean ± SEM, $^*p < 0.05$, $^{**}p < 0.01$

TET1-transfected iPSC-derived oligodendrocytes compared to control transfected cells (Fig. 7h). Overall, we observe more pronounced effects in the TET1-mediated demethylation experiments compared to DNMT3a-driven targeted methylation. In line, we observed a trend towards lower methylation levels and higher expression levels of *MBP* after targeted demethylation (Fig. 7i, j). Next to the low statistical power, our heterogeneous bulk cultures consisted of both transfected as well as untransfected cells, leaving our expression and methylation results confounded by the background noise of unmodified cells. Off note, the functional read-outs, which were based on transfected cells only, showed strong and significant results after epigenetic editing of *MBP* (Fig. 7a–h).

Discussion

In the current study, we investigated the transcriptomic and epigenomic profile of chronically demyelinated lesions and the surrounding NAWM from nine donors, with the final

goal of understanding the molecular mechanisms underlying the hampered differentiation capacity of OPCs within the MS lesion microenvironment. We found 641 genes to be differentially expressed between lesions and NAWM. Subsequent methylation analysis on this gene set revealed a total of 8336 CpGs located on 512 different genes displaying differential methylation between lesions and NAWM. Gene ontology analysis revealed enriched clusters of genes related to glial cell development and myelination. We then further explored *MBP*, the gene with the highest number of DMPs within the promotor region amongst these clusters. This gene displayed decreased expression as well as hypermethylation in lesions. Cell-specific validation of *MBP* methylation in lesion-derived OPCs revealed a similar hypermethylated profile compared to NAWM-derived OPCs. Finally, we functionally validated the influence of *MBP* methylation on oligodendrocyte differentiation by means of epigenetic editing.

The involvement of DNA methylation in oligodendrocyte differentiation has been investigated previously by us and other researchers [36, 45, 48, 49]. Using rodent-derived OPCs or mouse models for MS, it has been shown that the presence of DNA methylation enzymes, such as DNMT1 and DNMT3a, is crucial for oligodendrocyte differentiation during development and remyelination [36, 37]. Furthermore, we have recently established that the myelin regulatory pathway, *Id2* and *Id4* in particular, is under epigenetic control during physiological OPC differentiation [48]. Yet, the direct impact of DNA methylation in relation to remyelination failure in MS remained to be investigated. One of the first studies to use an epigenome-wide approach investigated methylomic alterations within NAWM brain samples of MS patients and compared them to matched non-neurological white matter control samples [23]. Pathology-free MS samples show differentially methylated regions within genes related to oligodendrocyte development and survival. In line with this notion, recent studies by Kular et al. showed specific DNA methylation profiles of neuronal and glial cells isolated from the NAWM of post-mortem MS brains [28, 30]. As for lesions, one study has investigated the difference in the methylation patterns between demyelinated and intact hippocampi of progressive MS patients using the Illumina Methylation 450K array. Chomyk et al. elegantly highlighted several DMPs related to neuronal survival and memory function yet did not reveal any methylation changes related to oligodendrocyte biology [9]. Altogether, it is evident that the DNA methylation is affected in MS post-mortem brain tissue, but how this relates to the block on OPC differentiation in chronically demyelinated lesions has remained unclear up to now.

In the present study, we aimed to investigate the methylomic signature of chronically demyelinated MS lesions to understand the direct contribution of DNA methylation to the hampered differentiation state of OPCs within these lesions. One of the main strengths of this study is the unique within-comparison between lesions and their surrounding NAWM isolated from each patient. This setup increased our statistical power and allowed us to investigate DNA methylation changes specifically related to the lesion microenvironment, where OPC differentiation is hampered. Furthermore, we examined both transcription and DNA methylation in these samples, allowing us to directly correlate our transcriptional data to the methylation profile of these genes. In our previous study, we identified *Id2* and *Id4* as important targets of DNA methylation during OPC differentiation into oligodendrocytes [48]. In the current dataset, however, these genes did not pass the FDR correction after DE analysis, and could therefore not be included in our methylation analysis. As we have previously shown that there were no significant differences in *Id2*/*Id4* methylation between lesions and NAWM [48], we do believe that our current analysis approach did not miss out on important findings regarding these genes.

Our GO analysis based on genes that displayed both differential expression and methylation, as well as a significant correlation between these two features, revealed two main clusters, i.e., 'cytoskeleton organisation' and 'glial cell development and myelination'. Genes within the latter cluster ranged from important myelin genes (*MBP, MAG*) and genes that regulate myelin formation (*CNTN2*, *LPAR1*) or OPC differentiation (*PARD3*, *BCAS1*), to genes important for lipid metabolism (*UGT8*, *ABCA2*) [12, 13, 15, 22, 47, 53]. Intriguingly, we found *MBP* to contain both the highest number of DMPs overall and the highest number of DMPs located within the promotor region and on CpG islands or shores. Moreover, all the probes within the promotor region of *MBP* were consistently hypermethylated in lesions compared to the surrounding NAWM. One could advocate that the *MBP* gene would be an obvious suspect to be altered within a demyelinated lesion. Interestingly, *MBP* has also been shown to be hypermethylated in NAWM samples of MS patients compared to non-neurological controls [23]. These findings suggest a possible step-wise methylation change in the *MBP* gene, already initiated in NAWM regions and becoming more pronounced in the actual lesion site, where myelin damage has already occurred. Interestingly, Kular et al. also observe differential methylation of two CpG sites within the *MBP* gene in glial nuclei sorted from MS patients [28]. These CpG sites are located in the gene body, whilst as we mainly focussed on the CpG sites within the promotor region to be able to directly link it to the expression of the gene. Nevertheless, it is very interesting to observe that *MBP* methylation is affected in MS samples, both in CI lesions and NAWM, in three independent datasets. Moreover, *MBP* has also been shown to be differentially methylated in other neurodegenerative diseases with white matter

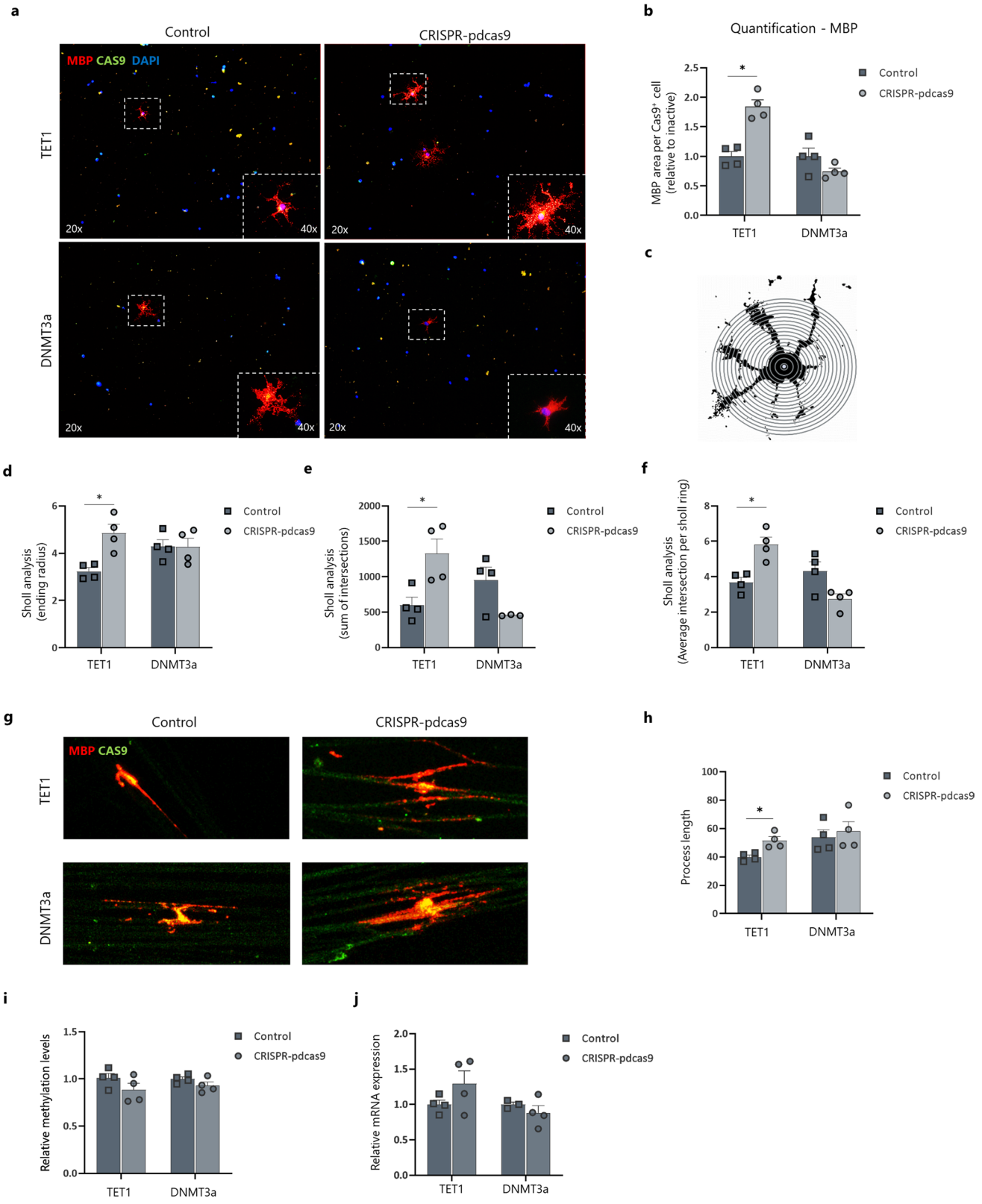

pathology, such as Alzheimer's disease (AD). A recent meta-analysis, which combined data from six independent brain AD methylation studies ($n = 1453$ individuals), investigated the methylation profile of 485,000 CpG sites, of which one of the differentially methylated CpG sites in the prefrontal cortex reaching genome-wide significance was located

◂**Fig. 7** Epigenetic editing of the *MBP* promotor region in human iPSC-derived oligodendrocytes influences the differentiation and myelination capacity. Human iPSC-derived oligodendrocytes were transfected with either a CRISPR–pdCas9-DNMT3a or CRISPR–pdCas9-TET1 vector to methylate or demethylate the promotor region of the *MBP* gene. Inactive constructs harbouring a catalytical inactive DNMT3a or TET1 were used as control. **a** Representative images of transfected human iPSC-derived oligodendrocytes. **b** Quantification (MBP fluorescence area) of transfected human iPSC-derived oligodendrocytes shows an effect on MBP protein expression after epigenetic editing ($n=4$, Wilcoxon test). **c**–**f** Representation and quantification of the Sholl analysis of transfected iPSC-derived oligodendrocytes ($n=4$, Wilcoxon test). **g**, **h** Confocal images and quantification showing increased formation of myelin-like extensions on microfibers after targeted demethylation of the *MBP* promotor ($n=4$, Wilcoxon test). **i** Methylation analysis of the *MBP* promotor region after epigenetic editing of the *MBP* promotor ($n=4$). **j** Gene expression analysis showed a tendency towards an altered expression profile of *MBP* after targeted (de)methylation. Data are corrected for the most stable housekeeping genes (RPL13a and TBP) ($n=4$). Data are represented as mean ± SEM, $^*p<0.05$

within the *MBP* gene [46]. Altogether, this emphasises the importance of DNA methylation in the regulation of *MBP* expression and its susceptibility to changes during disease. We should note, however, that other myelin genes, such as *MOG* and *MOBP*, also showed both differential expression as well as differential methylation, yet did not fall within the GO clusters in our analysis. These genes could still represent biological relevant targets for further investigation.

The observed hypermethylated profiles of *MBP* within NAWM and MS lesions represent interesting independent observations, yet they could potentially be explained by differences in cellular composition between patients and controls and between lesions and NAWM, respectively [23]. We, however, hypothesised that the epigenetic block on *MBP* was present in OPCs within lesions, thereby inhibiting their differentiation into myelin-forming oligodendrocytes. As such, we laser-captured OPCs both from lesions as NAWM samples and performed bisulfite pyrosequencing of the *MBP* promotor region. Altogether, these results indicate that the *MBP* promotor becomes hypermethylated in OPCs located within the lesion microenvironment, possibly preventing them from differentiating into mature oligodendrocytes. Indeed, in vitro experiments using OPCs isolated from *shiverer* mutant mice showed that the lack of *MBP* does not impact their proliferative capacity, but prevents their differentiation process towards mature oligodendrocytes [44]. Whilst the absence of other myelin proteins, such as PLP and CNP, does not affect CNS myelination, the lack of functional *MBP* results in severe myelination deficits [26, 38]. Next to its crucial role in myelin compaction, MBP also facilitates glial cytoskeleton assembly during oligodendrocyte differentiation. OPC undergoes major morphological changes during their differentiation into oligodendrocytes, which requires microfilament and microtubule network remodelling [18]. MBP has been shown to polymerise and bundle actin filaments and microtubules, cross-link them to each other, and facilitate their binding to the lipid membrane [6, 7, 19, 20]. In line, oligodendrocyte cultures derived from *shiverer* mice fail to form proper myelin sheaths due to abnormally assembled microtubule and actin-based structures, thereby emphasising the essential role of MBP during oligodendrocyte differentiation [11, 18]. Interestingly, next to the myelin cluster, we also observed an enriched GO cluster related to cytoskeleton organisation and actin-filament processes in our current dataset.

Our observations regarding *MBP* methylation in MS lesions and lesion-derived OPCs are novel, yet remain correlational. As we have suggested previously, it is important to investigate the potential cause-and-effect relationship between epigenetic signatures and functional read-outs, such as oligodendrocyte differentiation [25]. Over the past years, epigenetic editing, using CRISPR–dCas9 engineered systems, has proven to be a powerful tool to provide evidence of functional consequences of epigenetic changes at specific loci [51]. In the present study, we made use of both a CRISPR–dCas9-TET1 and a CRISPR–dCas9-DNMT3a vector to target and demethylate or methylate, respectively, the *MBP* promotor region with the final aim of assessing the influence on oligodendrocyte differentiation capacity [27, 50]. We used two cell culture models, i.e., human iPSC-derived oligodendrocytes and HOG cells, which we transfected with the epigenetic editing vector to target the *MBP* gene, and assessed the effects on MBP protein expression, cellular morphology, and myelination capacity. As a control for transfection and steric hindrance, we transfected cells with a catalytic inactive version of the vectors that are unable to (de)methylate. Interestingly, we observed significant functional effects after targeted demethylation of the *MBP* gene, resulting in higher MBP expression, a more differentiated cellular morphology, as well as an increased myelination capacity. Targeted methylation showed less-pronounced effects, yet did reveal a consistent trend towards reduced MBP protein expression and lower cellular complexity. A possible explanation for this could be that the baseline default methylation status of both cell culture types already levelled around 80%, leaving little room for effects of additional (hyper)methylation by the CRISPR–dCas9-DNMT3a vector. A limitation of the CRISPR–dCas9-based epigenetic editing tool is the possible off-target effects due to undesired binding to other genomic regions. The endonuclease inactive CRISPR–dCas9-based epigenetic editing tool acts mainly as a cargo protein to guide the effector domains to the desired region, and is therefore more tolerant to mismatches between the sgRNA and the DNA loci [33]. As we cannot completely rule out possible off-target events, we designed our sgRNA in such way that the predicted off-target sites were located in non-coding genomic regions.

Current study is based on the transcriptomic and epigenomic analysis of post-mortem brain tissue. A limitation here is that the integrity of the RNA is not optimal in such tissue, reflected by the RIN values. Hence, only samples with a RIN value above 2 were included in the transcriptomic analysis, yielding a limitation of this study. Furthermore, the limited sample size did not provide sufficient power to start the analyses with the DNA methylation dataset to explore associated genome-wide changes. However, in view of a more direct effect of transcriptomics on cellular biology, compared to methylation, we opted to start with the transcriptomic dataset and only investigated the methylation profile of the DE genes, yielding us relevant and interesting findings for further analysis.

Conclusion

Collectively, our data demonstrate strong differences in DNA methylation between chronically demyelinated MS lesions and the NAWM, which furthermore correlate with the expression profile of the corresponding DEGs. We identified an epigenetic block on *MBP* within OPCs located in the lesions and showed that this could have a major impact on the differentiation and myelination capacity of these cells. Notably, more than 8000 CpG sites displayed differential methylation within MS lesions, with numerous of them potentially impacting upon cellular behaviour within the lesion site. It is therefore important to further characterise MS-associated epigenetic signatures, preferably in a cell-type-specific manner, to fully understand the contribution of DNA methylation to remyelination failure in progressive MS stages. Which specific molecules and factors within the microenvironment of demyelinated lesions drive the observed epigenetic changes remains to be elucidated. Our study represents a starting point for important research regarding DNA methylation signatures in chronic MS lesions with the final aim to discover new targets to restore the remyelination capacity during progressive MS.

Supplementary Information The online version contains supplementary material available at https://doi.org/10.1007/s00401-023-02596-8.

Author contributions TV and DvdH designed and monitored the study. AT took the lead in performing the experiments, analysing and interpretation of the data, with critical input of RR, ED, CV, JP, EP, and NH. MS, LvV, SC, BR, and KW assisted in performing the experiments. AT, TV, and DvdH drafted the manuscript. All the authors revised the manuscript and agreed to the final version of the manuscript.

Funding This work was financially supported by grants from the Research Foundation of Flanders (FWO Vlaanderen; 1S25119N) and the Charcot Foundation of Belgium. The funding agencies have no role in the design, analysis, and writing of the article.

Data availability The Illumina EPIC and RNA sequencing data that support the findings of this study are openly available in the GEO Gene Expression Omnibus (GEO) database under the accession number GSE224457.

Declarations

Conflict of interest The authors declare that they have no competing interests.

Ethics approval and consent to participate All experiments on human post-mortem brain tissue were approved by the Hasselt University Medical Ethical Committee.

References

1. Andrews S (2010) FastQC: a quality control tool for high throughput sequence data. http://www.bioinformatics.babraham.ac.uk/projects/fastqc
2. Aronesty E (2011) ea-utils: command-line tools for processing biological sequencing data. https://github.com/ExpressionAnalysis/ea-utils
3. Aryee MJ, Jaffe AE, Corrada-Bravo H, Ladd-Acosta C, Feinberg AP, Hansen KD et al (2014) Minfi: a flexible and comprehensive Bioconductor package for the analysis of Infinium DNA methylation microarrays. Bioinformatics 30:1363–1369. https://doi.org/10.1093/bioinformatics/btu049
4. Bechler ME (2019) A neuron-free microfiber assay to assess myelin sheath formation. Methods Mol Biol 1936:97–110. https://doi.org/10.1007/978-1-4939-9072-6_6
5. Berry K, Wang J, Lu QR (2020) Epigenetic regulation of oligodendrocyte myelination in developmental disorders and neurodegenerative diseases. F1000Res. https://doi.org/10.12688/f1000research.20904.1
6. Boggs JM, Rangaraj G, Heng YM, Liu Y, Harauz G (2011) Myelin basic protein binds microtubules to a membrane surface and to actin filaments in vitro: effect of phosphorylation and deimination. Biochim Biophys Acta 1808:761–773. https://doi.org/10.1016/j.bbamem.2010.12.016
7. Boggs JM, Rangaraj G, Hill CM, Bates IR, Heng YM, Harauz G (2005) Effect of arginine loss in myelin basic protein, as occurs in its deiminated charge isoform, on mediation of actin polymerization and actin binding to a lipid membrane in vitro. Biochemistry 44:3524–3534. https://doi.org/10.1021/bi0473760
8. Celarain N, Tomas-Roig J (2020) Aberrant DNA methylation profile exacerbates inflammation and neurodegeneration in multiple sclerosis patients. J Neuroinflammation 17:21. https://doi.org/10.1186/s12974-019-1667-1

9. Chomyk AM, Volsko C, Tripathi A, Deckard SA, Trapp BD, Fox RJ et al (2017) DNA methylation in demyelinated multiple sclerosis hippocampus. Sci Rep 7:8696. https://doi.org/10.1038/s41598-017-08623-5
10. Dansu DK, Sauma S, Casaccia P (2021) Oligodendrocyte progenitors as environmental biosensors. Semin Cell Dev Biol 116:38–44. https://doi.org/10.1016/j.semcdb.2020.09.012
11. Dyer CA, Phillbotte T, Wolf MK, Billings-Gagliardi S (1997) Regulation of cytoskeleton by myelin components: studies on shiverer oligodendrocytes carrying an Mbp transgene. Dev Neurosci 19:395–409. https://doi.org/10.1159/000111237
12. Dzięgiel P, Owczarek T, Plazuk E, Gomułkiewicz A, Majchrzak M, Podhorska-Okołów M et al (2010) Ceramide galactosyltransferase (UGT8) is a molecular marker of breast cancer malignancy and lung metastases. Br J Cancer 103:524–531. https://doi.org/10.1038/sj.bjc.6605750
13. Fard MK, van der Meer F, Sánchez P, Cantuti-Castelvetri L, Mandad S, Jäkel S et al (2017) BCAS1 expression defines a population of early myelinating oligodendrocytes in multiple sclerosis lesions. Sci Transl Med. https://doi.org/10.1126/scitranslmed.aam7816
14. Franklin RJ, Ffrench-Constant C (2008) Remyelination in the CNS: from biology to therapy. Nat Rev Neurosci 9:839–855. https://doi.org/10.1038/nrn2480
15. García-Díaz B, Riquelme R, Varela-Nieto I, Jiménez AJ, de Diego I, Gómez-Conde AI et al (2015) Loss of lysophosphatidic acid receptor LPA1 alters oligodendrocyte differentiation and myelination in the mouse cerebral cortex. Brain Struct Funct 220:3701–3720. https://doi.org/10.1007/s00429-014-0885-7
16. Garcia-Leon JA, Garcia-Diaz B, Eggermont K, Caceres-Palomo L, Neyrinck K, Madeiro da Costa R et al (2020) Generation of oligodendrocytes and establishment of an all-human myelinating platform from human pluripotent stem cells. Nat Protoc 15:3716–3744. https://doi.org/10.1038/s41596-020-0395-4
17. Gruchot J, Weyers V, Göttle P, Förster M, Hartung H-P, Küry P et al (2019) The molecular basis for remyelination failure in multiple sclerosis. Cells 8:825. https://doi.org/10.3390/cells8080825
18. Harauz G, Boggs JM (2013) Myelin management by the 18.5-kDa and 21.5-kDa classic myelin basic protein isoforms. J Neurochem 125:334–361. https://doi.org/10.1111/jnc.12195
19. Hill CM, Harauz G (2005) Charge effects modulate actin assembly by classic myelin basic protein isoforms. Biochem Biophys Res Commun 329:362–369. https://doi.org/10.1016/j.bbrc.2005.01.151
20. Hill CM, Libich DS, Harauz G (2005) Assembly of tubulin by classic myelin basic protein isoforms and regulation by post-translational modification. Biochemistry 44:16672–16683. https://doi.org/10.1021/bi050646+
21. Houseman EA, Molitor J, Marsit CJ (2014) Reference-free cell mixture adjustments in analysis of DNA methylation data. Bioinformatics 30:1431–1439. https://doi.org/10.1093/bioinformatics/btu029
22. Hudish LI, Blasky AJ, Appel B (2013) miR-219 regulates neural precursor differentiation by direct inhibition of apical par polarity proteins. Dev Cell 27:387–398. https://doi.org/10.1016/j.devcel.2013.10.015
23. Huynh JL, Garg P, Thin TH, Yoo S, Dutta R, Trapp BD et al (2014) Epigenome-wide differences in pathology-free regions of multiple sclerosis-affected brains. Nat Neurosci 17:121–130. https://doi.org/10.1038/nn.3588
24. Kim D, Paggi JM, Park C, Bennett C, Salzberg SL (2019) Graph-based genome alignment and genotyping with HISAT2 and HISAT-genotype. Nat Biotechnol 37:907–915. https://doi.org/10.1038/s41587-019-0201-4
25. Koulousakis P, Tiane A, Hellings N, Prickaerts J, van den Hove D, Vanmierlo T (2023) A perspective on causality assessment in epigenetic research on neurodegenerative disorders. Neural Regen Res 18:331–332. https://doi.org/10.4103/1673-5374.343898
26. Krämer-Albers E-M, White R (2011) From axon–glial signalling to myelination: the integrating role of oligodendroglial Fyn kinase. Cell Mol Life Sci 68:2003–2012. https://doi.org/10.1007/s00018-010-0616-z
27. Kressler C, Gasparoni G, Nordström K, Hamo D, Salhab A, Dimitropoulos C et al (2020) Targeted de-methylation of the FOXP3-TSDR is sufficient to induce physiological FOXP3 expression but not a functional treg phenotype. Front Immunol 11:609891. https://doi.org/10.3389/fimmu.2020.609891
28. Kular L, Ewing E, Needhamsen M, Pahlevan Kakhki M, Covacu R, Gomez-Cabrero D et al (2022) DNA methylation changes in glial cells of the normal-appearing white matter in multiple sclerosis patients. Epigenetics. https://doi.org/10.1080/15592294.2021.2020436
29. Kular L, Jagodic M (2020) Epigenetic insights into multiple sclerosis disease progression. J Intern Med 288:82–102. https://doi.org/10.1111/joim.13045
30. Kular L, Needhamsen M, Adzemovic MZ, Kramarova T, Gomez-Cabrero D, Ewing E et al (2019) Neuronal methylome reveals CREB-associated neuro-axonal impairment in multiple sclerosis. Clin Epigenetics 11:86. https://doi.org/10.1186/s13148-019-0678-1
31. Leek JT, Johnson WE, Parker HS, Jaffe AE, Storey JD (2012) The sva package for removing batch effects and other unwanted variation in high-throughput experiments. Bioinformatics 28:882–883. https://doi.org/10.1093/bioinformatics/bts034
32. Li H, Handsaker B, Wysoker A, Fennell T, Ruan J, Homer N et al (2009) The Sequence Alignment/Map format and SAMtools. Bioinformatics 25:2078–2079. https://doi.org/10.1093/bioinformatics/btp352
33. Lin L, Liu Y, Xu F, Huang J, Daugaard TF, Petersen TS et al (2018) Genome-wide determination of on-target and off-target characteristics for RNA-guided DNA methylation by dCas9 methyltransferases. Gigascience 7:1–19. https://doi.org/10.1093/gigascience/giy011
34. Loma I, Heyman R (2011) Multiple sclerosis: pathogenesis and treatment. Curr Neuropharmacol 9:409–416. https://doi.org/10.2174/157015911796557911
35. McCartney DL, Walker RM, Morris SW, McIntosh AM, Porteous DJ, Evans KL (2016) Identification of polymorphic and off-target probe binding sites on the Illumina Infinium MethylationEPIC BeadChip. Genom Data 9:22–24. https://doi.org/10.1016/j.gdata.2016.05.012
36. Moyon S, Huynh JL, Dutta D, Zhang F, Ma D, Yoo S et al (2016) Functional characterization of DNA methylation in the oligodendrocyte lineage. Cell Rep 15:748–760. https://doi.org/10.1016/j.celrep.2016.03.060
37. Moyon S, Ma D, Huynh JL, Coutts DJC, Zhao C, Casaccia P et al (2017) Efficient remyelination requires DNA methylation. eNeuro. https://doi.org/10.1523/eneuro.0336-16.2017
38. Müller C, Bauer N, Schäfer I, White R (2013) Making myelin basic protein—from mRNA transport to localized translation. Front Cell Neurosci. https://doi.org/10.3389/fncel.2013.00169
39. Neyrinck K, Garcia-Leon JA (2021) Single transcription factor-based differentiation allowing fast and efficient oligodendrocyte generation via SOX10 overexpression. Methods Mol Biol 2352:149–170. https://doi.org/10.1007/978-1-0716-1601-7_11
40. Pidsley R, Wong CCY, Volta M, Lunnon K, Mill J, Schalkwyk LC (2013) A data-driven approach to preprocessing Illumina 450K methylation array data. BMC Genom 14:293. https://doi.org/10.1186/1471-2164-14-293
41. Popescu BFG, Pirko I, Lucchinetti CF (2013) Pathology of multiple sclerosis: where do we stand? Continuum (Minneapolis, Minn) 19:901–921. https://doi.org/10.1212/01.CON.0000433291.23091.65

42. Ritchie ME, Phipson B, Wu D, Hu Y, Law CW, Shi W et al (2015) limma powers differential expression analyses for RNA-sequencing and microarray studies. Nucleic Acids Res 43:e47. https://doi.org/10.1093/nar/gkv007
43. Samudyata C-B, Liu J (2020) Epigenetic regulation of oligodendrocyte differentiation: from development to demyelinating disorders. Glia 68:1619–1630. https://doi.org/10.1002/glia.23820
44. Seiwa C, Kojima-Aikawa K, Matsumoto I, Asou H (2002) CNS myelinogenesis in vitro: myelin basic protein deficient shiverer oligodendrocytes. J Neurosci Res 69:305–317. https://doi.org/10.1002/jnr.10291
45. Shen S, Sandoval J, Swiss VA, Li J, Dupree J, Franklin RJM et al (2008) Age-dependent epigenetic control of differentiation inhibitors is critical for remyelination efficiency. Nat Neurosci 11:1024–1034. https://doi.org/10.1038/nn.2172
46. Smith RG, Pishva E, Shireby G, Smith AR, Roubroeks JAY, Hannon E et al (2021) A meta-analysis of epigenome-wide association studies in Alzheimer's disease highlights novel differentially methylated loci across cortex. Nat Commun 12:3517. https://doi.org/10.1038/s41467-021-23243-4
47. Tanaka Y, Yamada K, Zhou CJ, Ban N, Shioda S, Inagaki N (2003) Temporal and spatial profiles of ABCA2-expressing oligodendrocytes in the developing rat brain. J Comp Neurol 455:353–367. https://doi.org/10.1002/cne.10493
48. Tiane A, Schepers M, Riemens R, Rombaut B, Vandormael P, Somers V et al (2021) DNA methylation regulates the expression of the negative transcriptional regulators ID2 and ID4 during OPC differentiation. Cell Mol Life Sci 78:6631–6644. https://doi.org/10.1007/s00018-021-03927-2
49. Tiane A, Schepers M, Rombaut B, Hupperts R, Prickaerts J, Hellings N et al (2019) From OPC to oligodendrocyte: an epigenetic journey. Cells. https://doi.org/10.3390/cells8101236
50. Vojta A, Dobrinić P, Tadić V, Bočkor L, Korać P, Julg B et al (2016) Repurposing the CRISPR-Cas9 system for targeted DNA methylation. Nucleic Acids Res 44:5615–5628. https://doi.org/10.1093/nar/gkw159
51. Xie N, Zhou Y, Sun Q, Tang B (2018) Novel epigenetic techniques provided by the CRISPR/Cas9 system. Stem Cells Int 2018:7834175. https://doi.org/10.1155/2018/7834175
52. Zheleznyakova GY, Piket E, Marabita F, Kakhki MP, Ewing E, Ruhrmann S et al (2017) Epigenetic research in multiple sclerosis: progress, challenges, and opportunities. Physiol Genom 49:447–461. https://doi.org/10.1152/physiolgenomics.00060.2017
53. Zoupi L, Savvaki M, Kalemaki K, Kalafatakis I, Sidiropoulou K, Karagogeos D (2018) The function of contactin-2/TAG-1 in oligodendrocytes in health and demyelinating pathology. Glia 66:576–591. https://doi.org/10.1002/glia.23266
54. Zurawski J, Stankiewicz J (2018) Multiple sclerosis re-examined: essential and emerging clinical concepts. Am J Med 131:464–472. https://doi.org/10.1016/j.amjmed.2017.11.044

Authors and Affiliations

Assia Tiane[1,2,3] · Melissa Schepers[1,2,3] · Rick A. Reijnders[2] · Lieve van Veggel[1,2,3] · Sarah Chenine[1,2,3] · Ben Rombaut[1,2,3] · Emma Dempster[4] · Catherine Verfaillie[5] · Kobi Wasner[6] · Anne Grünewald[6,7] · Jos Prickaerts[2] · Ehsan Pishva[2,4] · Niels Hellings[3,8] · Daniel van den Hove[2,9] · Tim Vanmierlo[1,2,3]

✉ Tim Vanmierlo
tim.vanmierlo@uhasselt.be

Assia Tiane
assia.tiane@uhasselt.be

Melissa Schepers
melissa.schepers@uhasselt.be

Rick A. Reijnders
ra.reijnders@maastrichtuniversity.nl

Lieve van Veggel
lieve.vanveggel@uhasselt.be

Sarah Chenine
sarah.chenine@uhasselt.be

Ben Rombaut
ben.rombaut@uhasselt.be

Emma Dempster
e.l.dempster@exeter.ac.uk

Catherine Verfaillie
catherine.verfaillie@kuleuven.be

Kobi Wasner
kobiwasner@gmail.com

Anne Grünewald
anne.gruenewald@uni.lu

Jos Prickaerts
jos.prickaerts@maastrichtuniversity.nl

Ehsan Pishva
e.pishva@maastrichtuniversity.nl

Niels Hellings
niels.hellings@uhasselt.be

Daniel van den Hove
d.vandenhove@maastrichtuniversity.nl

1 Department of Neuroscience, Biomedical Research Institute, Faculty of Medicine and Life Sciences, Hasselt University, Hasselt, Belgium

2 Department Psychiatry and Neuropsychology, School for Mental Health and Neuroscience, Maastricht University, Maastricht, The Netherlands

3 University MS Center (UMSC) Hasselt, Pelt, Belgium

4 Institute of Biomedical and Clinical Sciences, University of Exeter Medical School, University of Exeter, Exeter, UK

5 Stem Cell Institute, Department of Development and Regeneration, KU Leuven, Leuven, Belgium

6 Luxembourg Centre for Systems Biomedicine, University of Luxembourg, Esch-sur-Alzette, Luxembourg

[7] Institute of Neurogenetics, University of Lübeck, Lübeck, Germany

[8] Department of Immunology and Infection, Biomedical Research Institute, Faculty of Medicine and Life Sciences, Hasselt University, Hasselt, Belgium

[9] Department of Psychiatry, Psychosomatics and Psychotherapy, University of Wuerzburg, Würzburg, Germany